Supporting Information

Mangeol et al. 10.1073/pnas.1107121108

SI Materials and Methods

Determination of the Number of Unfolded Bases from Force Versus Displacement Curves. ***rRNA.*** To ascertain that the last state observed in the force versus displacement curves corresponds to the fully unfolded molecule, we applied forces well above the range where drops occurred (e.g., over 20 pN); no further transitions were observed. We then deduced the number of unfolded bases in each intermediate state from the gain in length corresponding to the successive substeps. Straight lines are used to fit the portions of the force versus displacement curves that correspond to the different states of the RNA. The intersections of these lines with an horizontal line (corresponding to a fixed force) provide the lengths (l_i) of the substeps at this particular force (Fig. S2). Fixing the force insures that the total length of the RNA/DNA double-stranded handles, as well as the average increase in length per unfolded base, remains constant throughout the unfolding process. The force is chosen so that the corresponding horizontal line falls closest to the data points from all states (Fig. S2).

A point that should be taken into account when linking the length of the substeps to the number of unfolded bases is that the initial and all intermediate states carry (at least) one RNA helix, while the fully unfolded state is single-stranded. The total length of the RNA segment subject to unfolding thus equals the length difference between the last state and the first state minus the helix diameter d_h of 2.2 nm (value derived from the structure in ref. 1). Altogether, the number b_i of bases unfolded when the ith intermediate state is reached, is proportional to the ratio between the increase in length upon going from the fully folded state to the ith state, and the total length of the construct:

$$b_i = \frac{\sum_{k=1}^{i} l_k}{\sum_{k=1}^{n} l_k + d_h} N_0,$$

where n is the number of substeps and N_0 the total number of bases of the RNA to be unfolded.

The same procedure is used to determine the number of unfolded bases in the mutated rRNA case (Fig. 2*B*). Of note, in this case several local helices probably fold or unfold in parallel, and the relationship between the measured length and the exact number of unfolded bases is less accurate than with the wild-type rRNA fragment, because each helix formation or elimination induces a 2.2 nm shift corresponding to about six unfolded bases.

mRNA. To determine the number of unfolded bases (b_i) corresponding to state i in the mRNA case, we simply compared the length of the construct in state i to the one calculated from elasticity models of single-stranded RNA. The analysis is similar to the ones used in refs. 2 and 3. This method has not been used in the rRNA case because modeling the elasticity of single-stranded rRNA was less straightforward in this case (see section on elasticity models).

Mapping the Position of Intermediate States on the rRNA Structure. Given the structure of the subdomain 991–1,163 of 23S rRNA (http://www.rna.ccbb.utexas.edu; see Fig. 1*E*), the unfolding of the molecule is supposed to be sequential. Only at the branched tip of the structure can unfolding propagate either toward H43 or toward H44. Because H44 is less stable, we assume that it unfolds first. Therefore, we attributed the last intermediate state to the bottom of H43.

Free Energy Estimations from Force Measurements. ***The "close-to-equilibrium" hypothesis.*** When the trap displacement is slow and when the activation barriers associated with molecular transitions do not exceed a few kT, unfolding can happen close-to-equilibrium. An experimental indication of this situation is force flipping. After partial unfolding, the RNA occasionally refolds, unfolds again, etc., in a stochastic process induced by thermal motion.

Such behavior is observed on the wild-type rRNA construct, especially for the first and the last two substeps (Fig. S3). It is not seen with the second substep presumably because the number of unfolded bases is larger in this case. Force flips also occur in the presence of L20C but only for the first substep that involves about 9 base pairs (Fig. S6). Subsequent unfolding events occur out of equilibrium because the force reached is too high.

Close-to-equilibrium behavior is also seen with the mRNA construct for the last two steps in absence of protein (Fig. S7), corresponding to the unfolding of two small hairpins named S2 and S4 in Fig. 3*E*.

For those transitions where no flipping occurs, it is desirable to quantify how close-to-equilibrium the system is—obviously a difficult issue. One possibility is to estimate the effect of the loading rate on the most probable unfolding forces. This can be done with the help of a Kramers model, which is of course a simplification because it approximates a transition that involves the unfolding of several bases by a thermally excited crossing of a single energy barrier. When the rate of force increase (r; pN/s) exceeds a critical value (r_c), the most probable unfolding force is predicted to increase by $k_B T/\delta \ln(r/r_c)$, where δ is the gain in length corresponding to the transition studied (4). This increase in force is a rough measure of how far the system is from equilibrium. The critical rate of force increase r_c is given by $k_B T\ k_0/\delta$, where k_0, the attempt frequency, is the inverse of the dwell time and is related to the transition energy (E) by $k_0 = \mathrm{A}e^{-(\mathrm{E}/\mathrm{kT})}$. Now, from the force flipping shown in Fig. S3 (rRNA fragment, no L20) we can directly deduce typical values for the dwell times of the fully folded and first unfolded states (both are of the order of 200 ms) and hence for k_0. Knowing the transition energy, the value of A can then be obtained. From this value and the values of E and δ, we have calculated r_c and the force increase induced by the loading rate for all four transitions observed for the rRNA fragment without L20C, including the second transition where no flipping occurs. Given the values of r used in our measurements (i.e., 2.3–3.3 pN/s in the force range where transitions occur), we find that $r/r_c < 10$ in all four cases, with increases in force of 0.20 pN, 0.35 pN, 0.30 pN, and 0 pN, respectively. These force increases are small compared to the unfolding forces (several pN), indicating that nonequilibrium effects induced by the loading rates are limited. This conclusion is further supported by earlier experiments on DNA unzipping. At a stiffness similar to the one used here, only velocities well above 200 nm/s start affecting the force signal (5, 6), to be compared with the 50 nm/s value used here.

Free energy estimations. The data presented here yield a straightforward estimation of the free energy change when the unfolding of a RNA region occurs close to equilibrium. The total free energy (G) of the system (the trapped beads and the molecular construct) varies along the unfolding pathway, due to changes in its elastic energy (E_l) and in the free energy of RNA folding (G_{RNA}). During a substep, upon going from the initial (i) to the final (f) state, E_l decreases because of the force drop (even

if a small gain comes from the newly stretched single-stranded RNA), and G_{RNA} increases because of the unfolded base pairs. Close-to-equilibrium, the free energies of the two states, G_i and G_f, are similar within a few kT; in particular, when averaged over several measurements, $G_i = G_f$. Consequently, the free energy released from unfolding equals the mean difference in elastic energy before and after unfolding: $G_{RNA,f} - G_{RNA,i} = \langle E_{l,i} - E_{l,f} \rangle$. The latter difference is given by the area between the force *vs.* displacement curves of the two states, assuming elastic behavior (cf. Fig. S4*A*).

As described in the main text, this method has been applied to the first substep in rRNA unfolding with and without L20C (18.2 ± 3.2 and 36.5 ± 5.3 unfolded bases, respectively), and to the last two substeps in mRNA unfolding without L20C. We have also used it to evaluate the work necessary to unfold the rRNA region encompassing the L20C binding site, corresponding to the first 36 bases, in the presence of the protein. In this case, the elasticity of the construction with 36 unfolded bases was extrapolated from the curve observed without protein, because in the presence of L20C this intermediate state cannot be observed (Fig. S4*B*).

Elasticity Models for Double-Stranded and Single-Stranded Regions. As mentioned above, the estimation of the free energy changes during the structural transitions of the rRNA and mRNA fragments, and the assignment of the intermediate states in the case of the mRNA fragment, rely upon elasticity models. Although the DNA/RNA hybrids used as linkers differ in sequence and length between the rRNA and mRNA constructs, they exhibit similar force versus displacement curves and their behavior is modeled in the same way. In contrast, the rRNA and mRNA fragments show different elastic behavior.

We approximate the elasticity of the DNA/RNA hybrid by the Odijk solution of the worm-like chain model (7) (Fig. S10*A*). It gives the mean extension $\langle x \rangle$ of the molecule as a function of the applied force F:

$$\langle x \rangle = L_0 \left(1 - \frac{1}{2} \left(\frac{k_B T}{F l_p} \right)^{1/2} + \frac{F}{K} \right),$$

where L_0 is the crystallographic length ($L_0 = 1.65$ μm for the rRNA construct and $L_0 = 1.51$ μm for the mRNA construct), l_p the persistence length ($l_p = 47 \pm 1$ nm), K the elastic modulus ($K = 1{,}000 \pm 50$ pN) and T the temperature ($T = 302 \pm 1$ °K).

Modeling the elasticity of the unfolded RNA regions is a challenging issue, because theoretical and experimental evidence shows that such regions can present single-stranded helices that strongly affect elasticity, especially in the 0–40 pN force range (8, 9). To our knowledge, no currently available model can predict the elasticity of RNA with a complex sequence when single-stranded helices occur. For the mRNA fragment, we successfully used the function proposed by Marko and Siggia to interpolate the solution of the worm-like chain model (10)—i.e., the data were fitted with the following function giving the force F as a function of the mean length x of the RNA fragment:

$$F = \frac{k_B T}{l_{pRNA}} \left(\frac{1}{4(1 - x/L)} + \frac{x}{L} - \frac{1}{4} \right),$$

where L is the crystallographic length of the RNA (we take 0.6 nm per nucleotide) and l_{pRNA} its persistence length (1.5 ± 0.1 nm). As this function gives the force as a function of the extension of the single-stranded RNA, and the Odijk solution gives the extension of the double-stranded linkers as a function of force, we had to calculate them separately and add them numerically in order to finally obtain the elasticity of the construct when the RNA is unfolded. Fig. S10*B* shows typical fits used for identifying the different unfolded states of the mRNA fragment.

For the rRNA fragment, the curve obtained by combining the Odijk solution and the Marko–Siggia function deviates from the experimental data in the 2–15 pN range (black, dashed curve in Figure S10*A*), presumably because of single-stranded helical regions. To obviate this difficulty, we empirically added a Gaussian function to the Marko and Siggia function:

$$F = \frac{k_B T}{l_{pRNA}} \left(\frac{1}{4(1 - x/L)} + \frac{x}{L} - \frac{1}{4} \right) + F_0 \exp\left(-\frac{(x - x_0)^2}{\lambda^2} \right),$$

where L and l_{pRNA} have the same values as before, and F_0, x_0 and λ are the coefficients of the gaussian function. These three parameters correspond to the amplitude, position, and extension of the correction used. With $F_0 = 5 \pm 0.3$ pN, $x_0 = 57 \pm 2$ nm and $\lambda = 22 \pm 5$ nm, the function fits the data very well (Fig. S10*A*, red curve).

Free Energy Estimation from Secondary Structure Prediction Tools. The mfold software (http://mfold.rna.albany.edu) has been used to estimate the free energy associated with certain helices in the rRNA or mRNA fragments. This software gives free energies at 29 °C and 1 M NaCl. As we work at the same temperature but with different ionic conditions (see *Materials and Methods* in the main text), free energies had to be corrected for this difference in salinity. We applied the same correction as for a DNA molecule of identical sequence (replacing U by T) and structure under the same ionic concentrations (11).

Refolding Experiments. After stretching the rRNA and mRNA constructs to the point that the RNA is completely unfolded, we approached back the two beads at 50 nm/s and measured the force versus trap displacement during the refolding process.

In the case of the rRNA, the measurements showed that, whether L20C was present or not, refolding was only complete at forces below about 4 pN, since the unfolding and refolding curves only merge below this force (Fig. S5). Compared to unfolding curves, refolding curves showed no sharp transitions: Presumably, whereas unfolding is sequential for the nonmutated rRNA fragment (Fig. 1), this fragment refolds through many intermediate states close in energy. Moreover L20C did not influence this process: Refolding curves in the presence or absence of L20C are indistinguishable.

Like for the rRNA fragment, the refolding curves for the mRNA fragment were identical whether L20C was present or not. However, in contrast with the rRNA fragment, intermediate states were reproducibly observed in this case (Fig. S8).

Additional Information on the Biological System.

L20 and L20C. The interaction of L20 with its two targets, the 23S rRNA and the *rpmI-rplT* mRNA, has been studied for long as a model system in one of our laboratories, using both in vivo approaches and ensemble in vitro techniques. Among the gathered information, the following results are relevant to the present work.

NMR studies of L20 in solution only reveal the structure of the C-terminal half of the L20 protein, L20C (12). This domain adopts a globular structure that remains the same whether or not L20C carries the highly basic and hydrophilic N-terminal half (L20N), and whether or not L20C contacts its specific binding sites on the *rpmI-rplT* mRNA (13). L20N is not visible in these NMR studies, presumably because it is largely unstructured. X-ray studies reveal that even in the crystal L20N remains partially unstructured (14). Only in the ribosome does it organize into a long, irregular α-helix that contacts many positions from Domains I, II, and V of 23S rRNA, whereas L20C binds a

well-defined site in the 991–1,163 subdomain, at the H 40–41 junction (15, 16) (Fig. S1). The folding of L20N in the ribosome may be favored by the neutralization of its many basic residues by the negatively charged RNA. In vivo, L20N is essential for 50S assembly, and the isolated L20C even exert a toxic, dominant-negative effect (17). Presumably, the isolated L20C outcompetes the full-length L20 from its H 40–41 binding site, implying that they both recognize the same site. As for the role of L20 in ribosome assembly, a likely possibility is that L20C first attaches to its specific binding site on the 991–1,163 subdomain, and that L20N subsequently participates in the folding/organization of the rest of Domain II as well as Domain I and V.

Contrasting with ribosome assembly, the autoregulation of the *rpmI-rplT* translation by L20 does not require L20N: In vivo, L20C and the full-length L20 are equivalent in this respect (12, 17). In vitro, the two proteins recognize the same two identical sites on the translational operator (cf. Fig. 3*E*), as judged by the arrests in primer extension that are observed in their presence (17). However, although the K_d for L20C binding to these sites (and to the H 40–41 site) could easily be measured by fluorescence anisotropy (these K_d fall in the 10 nM range), the K_d for L20 could not be determined "because of the aggregation tendency of the full-length protein" (18).

Force measurements on an rRNA fragment as large and complex as the target of full-length L20—i.e., Domains I–V of 23S rRNA—are unlikely to yield transitions attributable to precise structural elements (19). Together with the aggregation tendency of the full-length protein, this point is the main reason why we focus here on the truncated protein L20C interacting with its small rRNA and mRNA targets.

Subdomain 991–1,163 and Ribosome Assembly. The subdomain 991–1,163 plays obviously an important role in ribosome function: For instance, the binding of L11 at the tip of this structure (H 43 and 44) (20) is probably essential for the proper folding of the whole GTPase associated center (21). Now, what is the role of this subdomain in ribosome assembly? The following discussion relies largely on the work of Nierhaus and colleagues (summarized in ref. 22) and on our recent contributions.

In the ribosome structure, L3, L6, L13, L11, L20, L21, L25, and L36 directly contact (distance ≤ 3 Å) the 991–1,163 subdomain, and L22 lies not far from it (Fig. S1). Remarkably, four of these proteins (L3, L13, L20, and L22) lie among the six r-proteins that appear to bind 23S rRNA earliest during in vitro reconstitution experiments (22). The remaining two of these six early binders—i.e., L4 and L24—bind to a distant region (nt 298–340 from Domain I) (23). In view of the early binding of L3, L13, L20, and L22, it is possible that the 991–1,163 subdomain and associated proteins can fold on their own and then assists the folding of other rRNA regions. Indeed, the proteins that bind the 991–1,163 subdomain are also in contact with all other rRNA domains: L3 with Domains IV–V–VI, L6 with Domain VI, L13, L20, L21, and L25 with various regions of Domain I and/or II (as well as Domain VI for L13 and IV for L20), L36 with domains V and VI. However, it is more plausible that the folding of the 991–1,163 subdomain is only secondary to that of the region bound by L4 and L24. Indeed, it is thought that it is the binding of L24 to 23S rRNA that usually initiate the highly cooperative assembly process ("initiator protein"), with L20 only playing this role in the absence of L24 (22). Interestingly in this respect, we have recently obtained evidence that SrmB, a DEAD-box helicase that facilitates an early stage of the 50S assembly in vivo (24), binds the nascent subunit by recognizing the L4–L24 cluster (25), and subsequently assists the folding of the 991–1,163 subdomain, facilitating notably the incorporation of L13 (26).

1. Saenger W (1984) Principles of nucleic acid structure (Springer, New York).
2. Onoa B, et al. (2003) Identifying kinetic barriers to mechanical unfolding of the *T. thermophila* ribozyme. *Science* 299:1892–1895.
3. Greenleaf WJ, Frieda KL, Foster DA, Woodside MT, Block SM (2008) Direct observation of hierarchical folding in single riboswitch aptamers. *Science* 319:630–633.
4. Evans E (2001) Probing the relation between force—lifetime—and chemistry in single molecular bonds. *Annu Rev Biophys Biomol Struct* 30:105–128.
5. Bockelmann U, Thomen P, Essevaz-Roulet B, Viasnoff V, Heslot F (2002) Unzipping DNA with optical tweezers: High sequence sensitivity and force flips. *Biophys. J* 82:1537–1553.
6. Thomen P, Bockelmann U, Heslot F (2002) Rotational drag on DNA: A single molecule experiment. *Phys Rev Lett.* 88:248102.
7. Odijk T (1995) Stiff chains and filaments under tension. *Macromolecules* 28:7016–7018.
8. Buhot A, Halperin A (2004) Effects of stacking on the configurations and elasticity of single-stranded nucleic acids. *Phys Rev E Stat Nonlin Soft Matter Phys* 70:020902.
9. Seol Y, Skinner GM, Visscher K, Buhot A, Halperin A (2007) Stretching of homopolymeric RNA reveals single-stranded helices and base-stacking. *Phys Rev Lett* 98:158103.
10. Bustamante C, Marko JF, Siggia ED, Smith S (1994) Entropic elasticity of lambda-phage DNA. *Science* 265:1599–1600.
11. SantaLucia J Jr. (1998) A unified view of polymer, dumbbell, and oligonucleotide DNA nearest-neighbor thermodynamics. *Proc Natl Acad Sci USA* 95:1460–1465.
12. Raibaud S, et al. (2002) NMR structure of bacterial ribosomal protein l20: implications for ribosome assembly and translational control. *J Mol Biol* 323:143–151.
13. Raibaud S, et al. (2003) How bacterial ribosomal protein L20 assembles with 23 S ribosomal RNA and its own messenger RNA. *J Biol Chem* 278:36522–36530.
14. Timsit Y, Allemand F, Chiaruttini C, Springer M (2006) Coexistence of two protein folding states in the crystal structure of ribosomal protein L20. *EMBO Rep* 7:1013–1018.
15. Schuwirth B, et al. (2005) Structures of the bacterial ribosome at 3.5 A resolution. *Science* 310:827–834.
16. Selmer M, et al. (2006) Structure of the 70S ribosome complexed with mRNA and tRNA. *Science* 313:1935–1942.
17. Guillier M, et al. (2005) The N-terminal extension of *Escherichia coli* ribosomal protein L20 is important for ribosome assembly, but dispensable for translational feedback control. *RNA* 11:728–738.
18. Allemand F, Haentjens J, Chiaruttini C, Royer C, Springer M (2007) *Escherichia coli* ribosomal protein L20 binds as a single monomer to its own mRNA bearing two potential binding sites. *Nucleic Acids Res* 35:3016–3031.
19. Harlepp S, et al. (2003) Probing complex RNA structures by mechanical force. *Eur Phys J E* 12:605–615.
20. Wimberly B, Guymon R, McCutcheon J, White S, Ramakrishnan V (1999) A detailed view of a ribosomal active site: The structure of the L11-RNA complex. *Cell* 97:491–502.
21. Wilson D, Nierhaus K (2005) Ribosomal proteins in the spotlight. *Crit Rev Biochem Mol Biol* 40:243–267.
22. Nierhaus K (1991) The assembly of prokaryotic ribosomes. *Biochimie* 73:739–755.
23. Stelzl U, Nierhaus KH (2001) A short fragment of 23S rRNA containing the binding sites for two ribosomal proteins, L24 and L4, is a key element for rRNA folding during early assembly. *RNA* 7:598–609.
24. Charollais J, Pflieger D, Vinh J, Dreyfus M, Iost I (2003) The DEAD-box RNA helicase SrmB is involved in the assembly of 50S ribosomal subunits in *Escherichia coli*. *Mol Microbiol* 48:1253–1265.
25. Trubetskoy D, Proux F, Allemand F, Dreyfus M, Iost I (2009) SrmB, a DEAD-box helicase involved in *Escherichia coli* ribosome assembly, is specifically targeted to 23S rRNA in vivo. *Nucleic Acids Res* 37:6540–6549.
26. Proux F, Dreyfus M, Iost I (2011) Identification of the sites of action of SrmB, a DEAD-box RNA helicase involved in *Escherichia coli* ribosome assembly. *Mol Microbiol* 82:300–311.

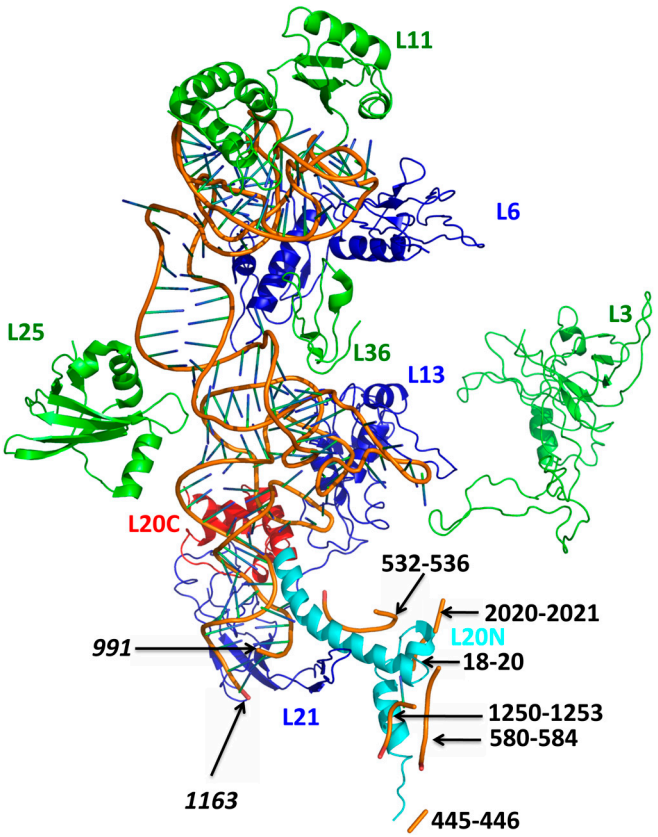

Fig. S1. Structure of the 991–1,163 subdomain from 23S rRNA in the *E. coli* ribosome showing the r-proteins that contact this subdomain and some of the other 23S rRNA regions that contact the N-terminal domain of L20, L20N (from PDB ID code 2I2V; we consider that two molecules are in "contact" if they come closer than 3 Å). Two different colors have been used for the two domains of L20 (L20N: blue; L20C: red). L20C is shown interacting with the H 40–41 junction within the 991–1,163 subdomain. In contrast L20N contacts rRNA regions from Domains I, II, and V. For clarity, only about half of these regions have been represented; the corresponding backbones and nucleotide coordinates are shown.

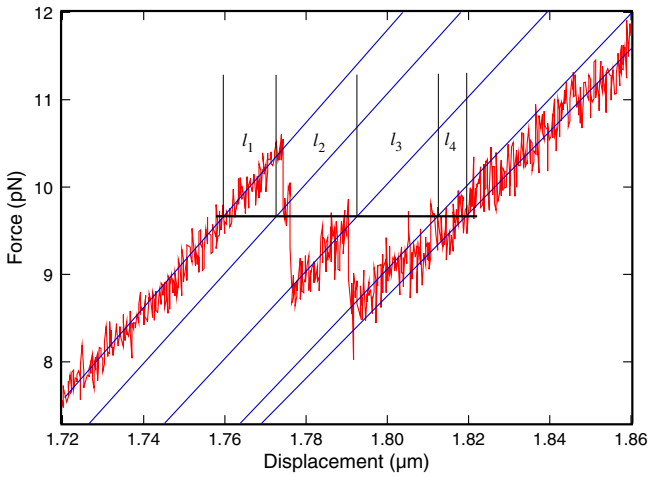

Fig. S2. Estimation of the length associated with the successive substeps during rRNA unfolding. Each blue line corresponds to one particular folded state. The lengths are measured from the intersections of these lines and a horizontal line corresponding to a constant force.

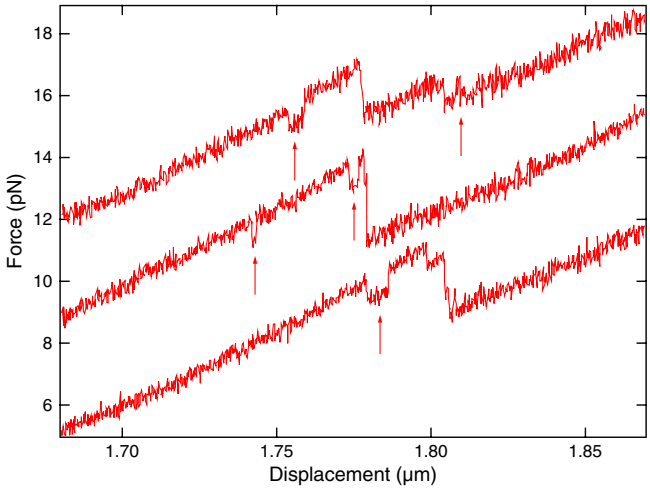

Fig. S3. Force flipping in stretching the rRNA fragment in the absence of L20C. Arrows point to transient, stochastic transitions between successive unfolded states; these transitions occur most often during the first substep. Three experiments are shown. For clarity, the two upper traces have been shifted upwards by 3 and 6 pN, respectively.

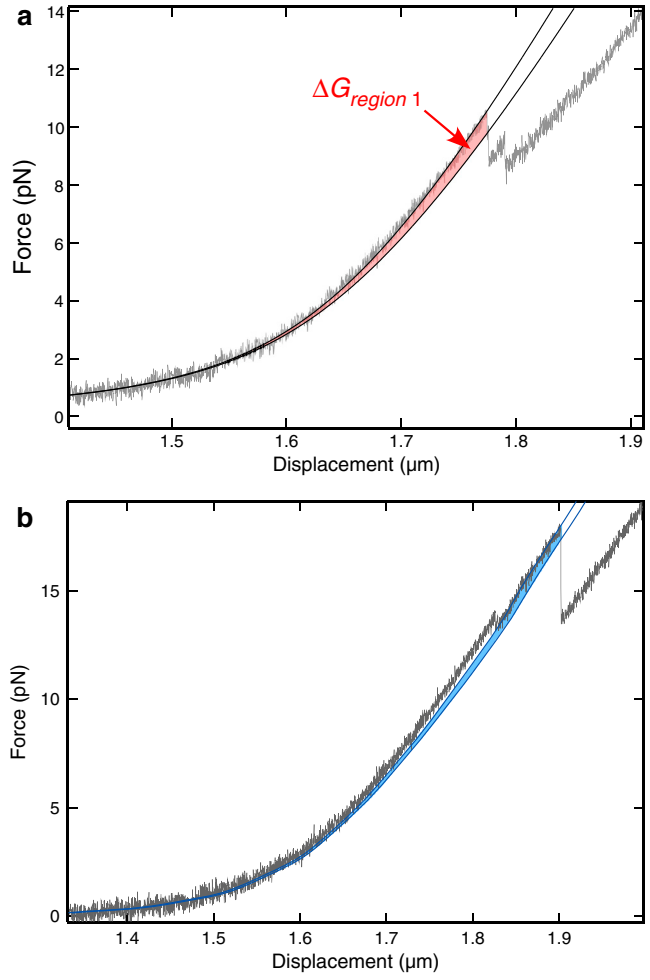

Fig. S4. Free energy changes associated with molecular transitions in the wild-type rRNA fragment. (*A*) Estimation of the free energy change between the fully folded state and the first intermediate state (36 unfolded bases) from a single force measurement curve. No L20C was present. The two black lines give the elasticity of the two states; the light red area gives the difference in elastic energy between them for the displacement at which the transition occurs. (*B*) Estimation of the free energy necessary to go from 18 to 36 unfolded bases (i.e., to unfold the binding site of L20C) in the presence of the protein. The two blue lines give the elasticity of the construction for the first intermediate state (18 unfolded bases) and for the state where 36 bases are unfolded. The latter line can be observed in the absence of L20C (see *A*). The free energy change is estimated from the area between the two lines for the displacement at which the transition occurs (pale blue area).

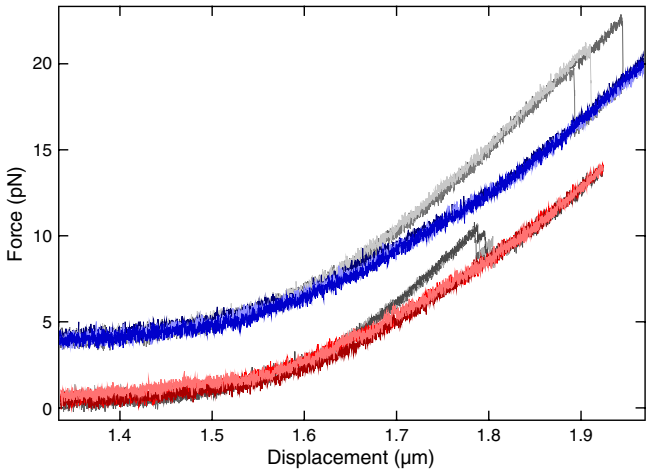

Fig. S5. Force measurements during the refolding of the rRNA fragment in the absence or presence of L20C. After complete RNA unfolding, the two beads were allowed to reapproach. Refolding traces with and without L20C are shown in blue and red, respectively. In both cases, different color tones correspond to three successive experiments with the same molecule. The corresponding unfolding traces are shown in gray, again with three different tones. For clarity, the traces obtained in the presence of L20C have been shifted upwards by 3.5 pN.

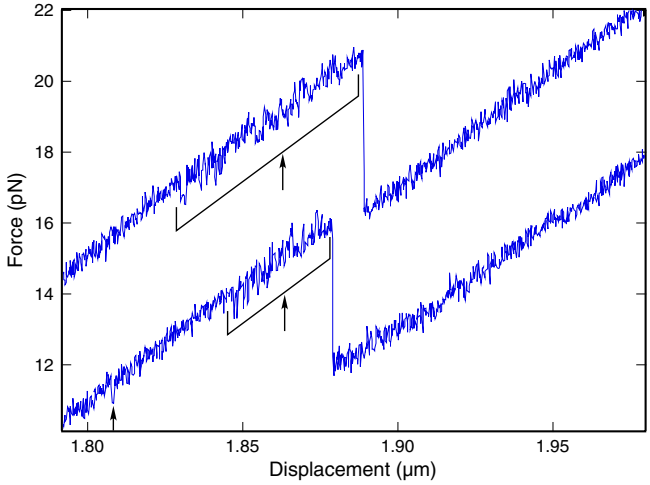

Fig. S6. Force flipping in stretching the rRNA construct in the presence of L20C. Arrows point to a force range where stochastic transitions between the fully folded state and the first intermediate state (18 unfolded bases) are observed. Two independent experiments are shown; for clarity, the upper trace has been shifted upwards by 4 pN.

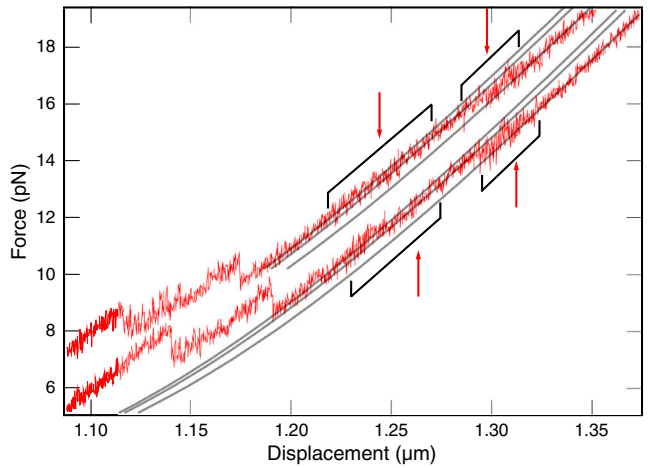

Fig. S7. Force flipping in stretching the mRNA construct in the absence of L20C. These transitions involve the last two intermediate states. Two independent traces are shown; for clarity, the upper one has been shifted upward by 2 pN. Red arrows point to regions where stochastic transitions between states are particularly frequent.

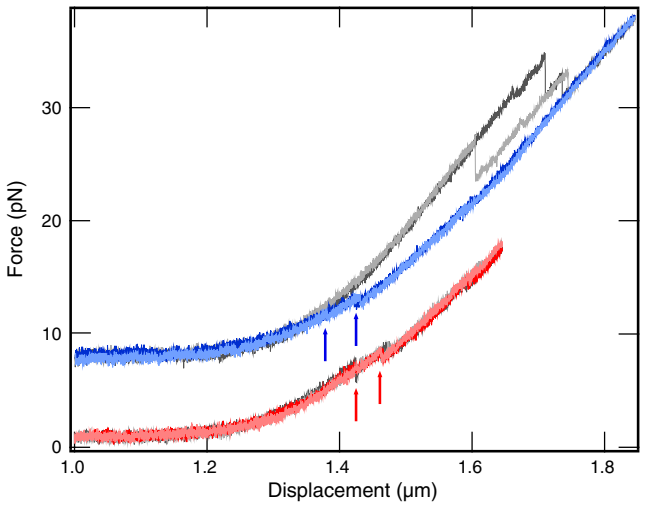

Fig. S8. Force measurements during the refolding of the mRNA fragment in the absence or presence of L20C. See legend of Fig. S5 for details. Note the presence of well-defined transitions during the refolding process (arrows). The traces corresponding to experiments in the presence of L20C have been shifted upward by 7 pN for better visualization.

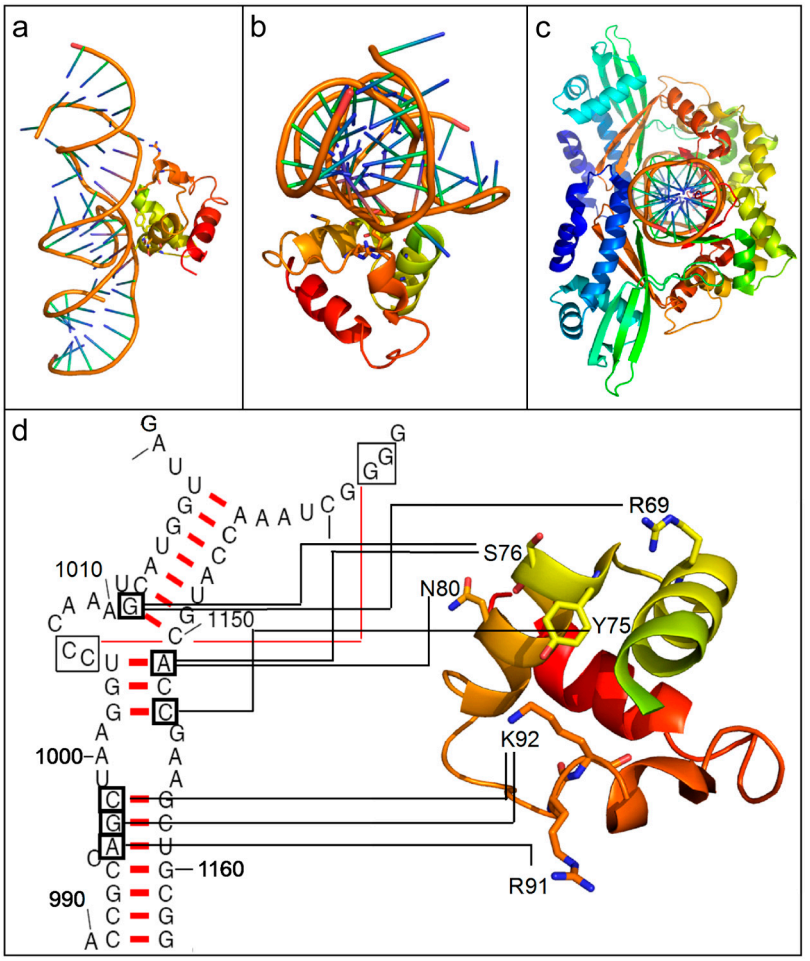

Fig. S9. Comparison of the 3D structures of the r-protein L20 (C-terminal half) with its 23S rRNA binding site, and of the restriction type II endonuclease *Bso*BI with its DNA recognition site. (*A* and *B*) Side and top view of L20C bound to the H 40–41 junction (PDB ID code 2I2V). (*C*) Top view of *Bso*BI bound to its recognition site (PDB ID code 1DC1). (*D*) Detail of the hydrogen bonds (black lines) between L20C and the H 40–41 junction (PDB ID code 2I2V). Only those L20C residues that are involved in H bonds are indicated; the corresponding nucleotides are squared. The tertiary interaction between nucleotides 1,005—1,006 and 1,138—1,137 is shown as a red line. Three-dimensional structures were drawn using Pymol (http://www.pymol.org/).

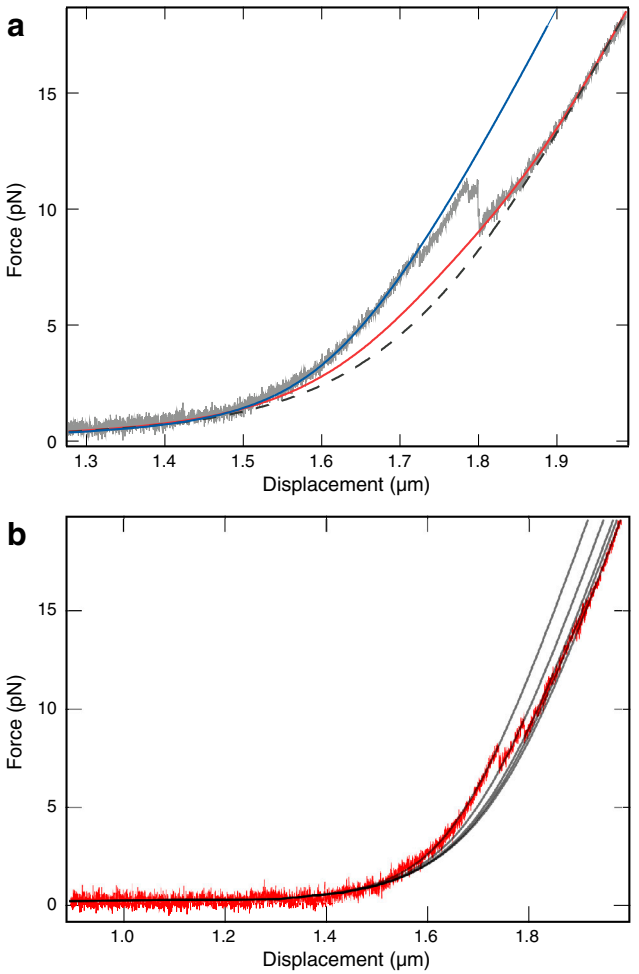

Fig. S10. Fitting the force versus displacement trace with elasticity models. (*A*) rRNA construct. The gray trace is a measurement done on the wild-type rRNA fragment in the absence of L20C. The blue curve is the Odijk solution for the worm-like chain model. It fits the measurements in the force range where the RNA remains completely folded (i.e., when the construct under tension is fully double-stranded). The black, dashed curve combines the Odijk solution with the model of Marko and Siggia for the elasticity of the single-stranded part of the construct. It fits the data at low and high force but fails to do so in the 2–14 pN range. The red curve, which is obtained by adding a Gaussian function to the Marko–Siggia formula (see *Elasticity Models for Double-Stranded and Single-Stranded Regions* above), fits the data over the entire force range. (*B*) mRNA construct. The trace shown (red) was obtained in absence of L20C. The elasticity of each intermediate (gray curves) is fitted by combining the Odijk solution with the model of Marko and Siggia for the double-stranded and single-stranded parts of the construct, respectively.